Supplemental Data

Incorporation of *Drosophila* CID/CENP-A and CENP-C into Centromeres during Early Embryonic Anaphase

Melina Schuh, Christian F. Lehner, and Stefan Heidmann

Supplemental Experimental Procedures

DNA Constructs

For the construction of a green fluorescent CID variant, the EGFP coding sequence was inserted into an internal position for the following reasons. Our previous studies have indicated that a C-terminally tagged CID variant is only partially functional. The fusion protein localizes to the centromere, but the corresponding transgene fails to complement the lethality associated with *cid* mutants (unpublished observation). Similar observations were described for a C-terminally fused mouse CENP-A-GFP construct [S1]. Moreover, the N terminus of CID is thought to be required for the recruitment of other kinetochore components. Thus, we left the free N terminus unscathed and inserted the EGFP coding region within the CID N-terminal tail (between the codons specifying amino acids 118 and 119), directly upstream of an 11 amino acid stretch that is conserved among various Drosophilids and which in all cases immediately abuts the histone fold domain [S2]. First, a 772 bp fragment encompassing 412 bp upstream of the *cid* translational initiation codon and 354 bp of the coding region up to codon 118 was PCR amplified with w^1 genomic DNA as template, the oligodeoxynucleotides DW4 (5′-CGG GGTACC CGACATGGCTGTATCTTCAG-3′) and DW10 (5′-CG C GGATCC GGTCTGGTTTTGCGCAGCA-3′), and the Long Range PCR amplification kit (Roche Biochemicals) according to the manufacturer's recommendations. A second fragment encompassing the EGFP coding region was amplified with *Pfu*-Polymerase, the plasmid pBac{3xP3-EGFPaf} [S3] as template, and the oligodeoxynucleotides DW6 (5′-CGC GGATCC GGCGGCGGCATGGTGAGCAAG GGCGAG-3′) and DW7 (5′-CCAC AAGCTT GCCGCCGCCCTTGTAC AGCTCGTCCATGC-3′). These oligodeoxynucleotides introduced restriction sites as well as three codons for glycine residues at both sides of EGFP to serve as flexible linker. The two PCR fragments were cleaved at the restriction sites introduced by the primers (underlined) and cloned simultaneously into pBluescript (Stratagene). A third fragment encompassing the *cid* region coding for amino acids 119 through 225 as well as 513 bp of the flanking 3′-genomic region was PCR amplified with w^1 genomic DNA as template, the oligodeoxynucleotides DW11 (5′-CCAC AAGCTT AGGCGGCG CAAAGCGGC-3′) and DW3 (5′-CTAG TCTAGA GGTGACTCATTTC AAAAAGCG-3′) and cloned simultaneously with the 5′-*cid-EGFP*-fused fragment isolated from the pBluescript clone into the transformation vector pCaSpeR4 [S4].

To obtain lines expressing the fly histone H2 variant His2Av fused to mRFP1 [S5], a construct very similar to that used by Clarkson and Saint [S6] for the expression of His2Av-GFP was assembled in Litmus 28 (New England Biolabs). First, a 2240 bp fragment encompassing 751 bp upstream of the *His2Av* translational initiation codon and the complete *His2Av* coding region up to the ultimate codon was PCR amplified with w^1 genomic DNA as template, the oligodeoxynucleotides SH141 (5′-GGT TCTAGA TCTCACCGAATCC TCC-3′) and SH142 (5′-GGTC ACCGGT CCGTAGGCCTGCGACAGA ATG-3′), and the Long Range PCR amplification kit. This fragment was cut with AgeI and XbaI and cloned into an equally cleaved Litmus 28. The mRFP1 coding region was amplified with the oligodeoxynucleotides SH146 (5′-GGTA ACCGGT CGATAAGGATCCGATGG-3′) and SH147 (5′-GCAGCCGGATC AAGCTT CG-3′) and pRSETB-mRFP1 (gift of R. Tsien, San Diego, CA) as template, and the resulting fragment was cloned in-frame as an AgeI/HindIII fragment downstream of the His2Av coding region. A 1690 bp fragment of genomic His2Av 3′-flanking DNA was amplified with the oligodeoxynucleotides SH143 (5′-GGA AAGCTT AAGCCAGTCGGCAATCGG-3′) and SH144 (5′-GGA ACTAGT AAGATCTGCTGGATGAGGAC-3′) and w^1 genomic DNA as template and was cloned downstream of the *His2Av-mRFP1*-fusion as a HindIII/SpeI fragment. The integrity of PCR-amplified protein coding regions was verified by DNA sequencing. The final assembled construct was excised as a 4630 bp BglII fragment and cloned into a BamHI cleaved transformation vector pCaSpeR4.

Strains allowing maternal expression of the *NLS-tetR-EGFP* fusion gene under control of the *nanos* (*nos*) promoter and with the α*1-tubulin* (α*1tub*) 3′-UTR were constructed as follows. First, the EGFP coding region was obtained as a BamHI/HindIII fragment from pCaSpeR4-EGFP-cid and cloned into Litmus28. Then, the *tetR* coding region including an N-terminal fused nuclear localization signal (NLS) was PCR amplified with as template the plasmid p128tetR-GFP, which had been shown to direct expression of *NLS-tetR-GFP* in yeast cells [S7]. The PCR product was cloned in-frame upstream of EGFP in Litmus28-EGFP. A 917 bp genomic fragment containing the 5′-UTR and upstream regulatory sequences of the *nos* gene as well as an 860 bp genomic fragment containing the 3′UTR and downstream flanking sequences of the α*1tub* gene were PCR amplified with the Long Range PCR amplification kit and w^1 genomic DNA as template. These two regions have been shown to direct maternal expression of transgenes throughout the early *Drosophila* embryo [S8]. The *nos* 5′ and α*1tub* 3′ PCR fragments were then cloned successively upstream and downstream of NLS-tetR-EGFP, respectively. PCR-amplified coding regions were verified by DNA sequence analysis. The final assembled construct was excised as a 3189 bp SpeI/Asp718 fragment and cloned into pCaSpeR4. 224 tandem copies of the *tet*-operator sequence were obtained as an 11.5 kb BamHI/BglII fragment from the plasmid p306tetO224 [S7] and were also cloned into pCaSpeR4.

Fly Strains

Transgenic *Drosophila* lines were obtained after P-element-mediated germline transformation according to standard procedures. Both *His2Av-mRFP1* and *EGFP-cid* were expressed under control of the respective genomic regulatory sequences. To assay whether the *EGFP-cid* transgene is functional, complementation assays were performed with the lethal null mutant alleles $cid^{T12\text{-}1}$ and $cid^{T22\text{-}4}$ [S9]. When provided by the mother, a single copy of the transgene insertion *EGFP-cid* III.2 complements the lethality associated with the transheterozygous *cid* null mutant situation $cid^{T12\text{-}1}$/$cid^{T22\text{-}4}$ with high efficiency (88% of expected; 1224 progeny scored). A rescue stock expressing exclusively *EGFP-cid* could be established with two copies of the *EGFP-cid* III.2 transgene insertion. The *His2Av-mRFP1* transgene is also functional as it complements the lethality associated with the hemizygous *His2Av* mutant situation $His2Av^{05146}$/*Df(3R)ro80b* (data not shown).

Strains expressing EYFP fused to *Drosophila* CENP-C (EYFP-CENP-C) [S10], the $Mps1^1$ allele [S11], as well as the generation of $Mps1^1$ germline clones to obtain eggs without maternal $Mps1^+$ contribution have been described previously [S11]. Strains expressing *His2Av-mRFP1* together with *EGFP-cid* or *EYFP-Cenp-C* in an $Mps1^1$ heterozygous mutant background appropriate for germline clone production were constructed with standard genetic techniques. *His2Av* and *cid* mutant strains to test the biological functionality of the transgenes were obtained from the Bloomington *Drosophila* stock center or were kindly provided by T. Kaufman, respectively.

Among the *tetop* transgenic lines, a double insertion on the third chromosome (line *tetop* III.1/*TM3, Ser*) allowed observation of GFP dots in living syncytial embryos with the best signal-to-noise ratio.

In Vivo Imaging

Embryos expressing *His2Av-mRFP1* alone or in combination with *EGFP-cid* or *EYFP-Cenp-C* were obtained and prepared as described previously [S12]. After ageing to the appropriate stage under halocarbon oil, embryos were observed while progressing through epidermal mitoses 10–13. Nonsaturated images were acquired every 15 s with an inverted Leica DM-IRBE/TCS SP1 confocal system equipped with a 40×/1.25 oil immersion objective. For the FRAP

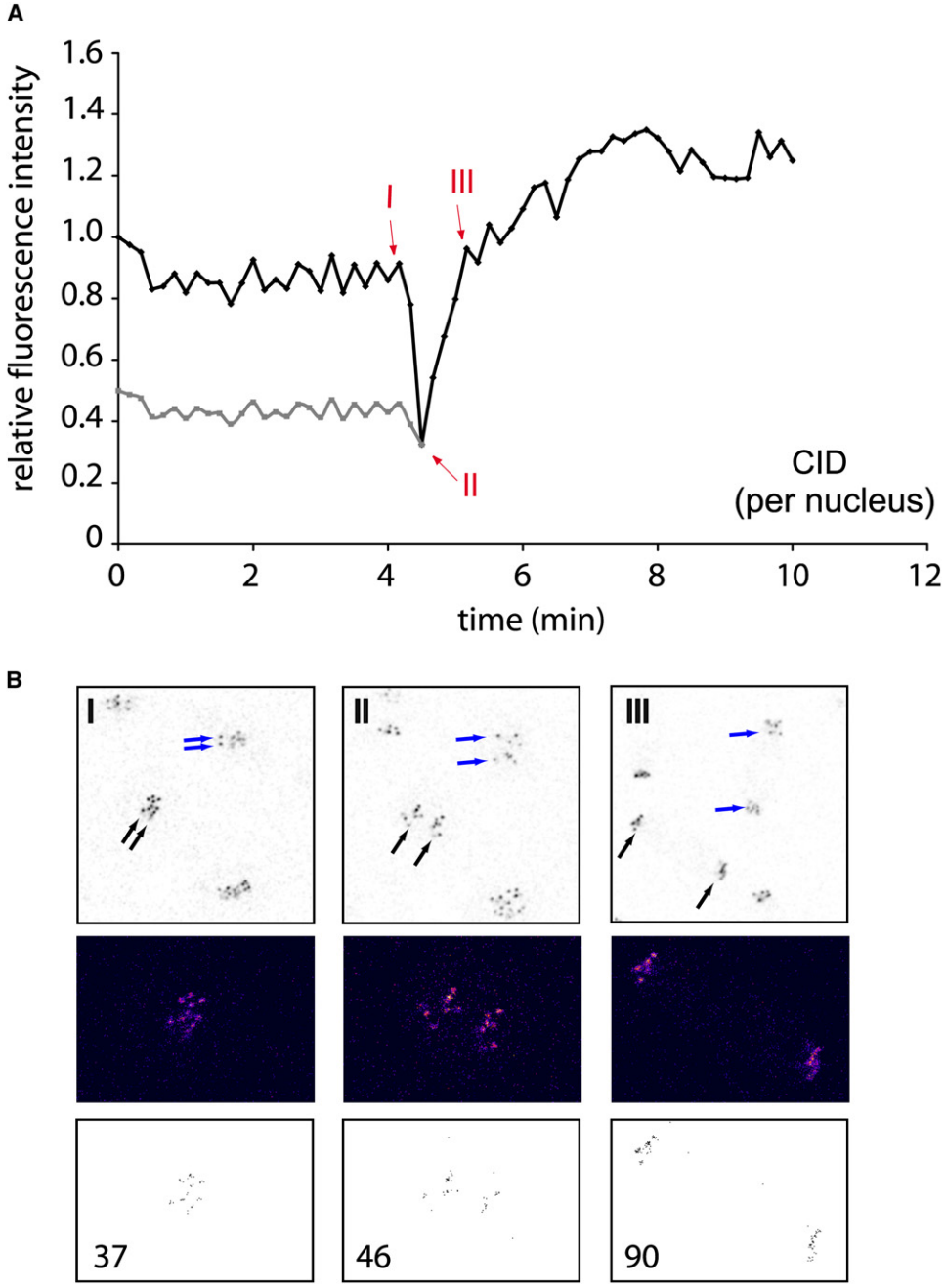

Figure S1. Incorporation of EGFP-CID during Anaphase in a *cid* Mutant Background

(A) Living embryos expressing exclusively *EGFP-cid* in a transheterozygous *cid* mutant background (line $cid^{T12\text{-}1}/cid^{T22\text{-}4}$; *EGFP-cid* III.2/*EGFP-cid* III.2) were observed while progressing through mitosis 11. Images were acquired in 10 s intervals. The fluorescence intensity of EGFP-CID in a total of 14 selected nuclei was determined for each frame. Data sets from two embryos were aligned according to the first frame indicating the onset of anaphase (labeled II). The fluorescence intensities of interphase nuclei were normalized to 100% at the start of image acquisition. The graph represents the average values obtained in the two experiments. The gray line in the graph indicates the calculated fluorescence intensities of individual sister centromere groups per nucleus before their actual evaluation is possible, obtained by halving the measured intensities at these time points.

(B) Images corresponding to selected time points (indicated by arrows numbered with roman numerals in [A]) of one of the series. The pixel values have been reversed for clarity. Arrows indicate groups of centromeric signals belonging together. The actual frames used for data evaluation were 4 times the area of the frames illustrated in the figure. The enlargements are shown for clarity. One mitotic figure has been enlarged even further and the increase in pixel intensity during anaphase is illustrated by a false color representation ([B], middle). The same mitotic figure is shown in a binary representation in the bottom panel with only those pixels displayed that have a value above 70. The actual pixel numbers are given in the lower left corners. The increase during anaphase of the number of pixels above the threshold of 70 is obvious.

experiments and the evaluation of single centromeres, an upright Zeiss LSM510 confocal system equipped with a 63×/1.40 oil immersion objective was used. Both confocal systems were equipped with 488 nm Ar lasers and 543 nm He/Ne lasers for the excitation of EYFP/EGFP and mRFP1, respectively. To allow for gas exchange when using the upright Zeiss microscope, we placed the immobilized

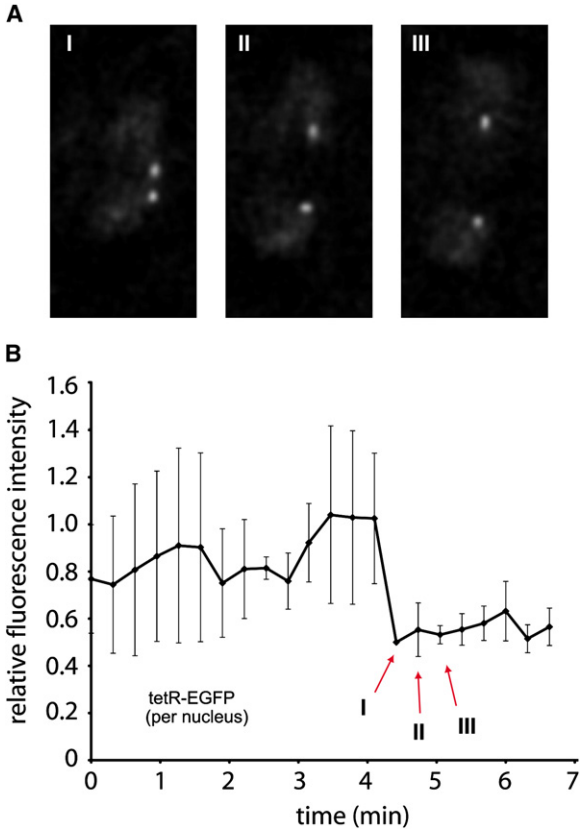

Figure S2. The Fluorescence Intensity of tetR-EGFP Fusion Proteins Bound to Chromosomally Integrated *tet*-Operator Arrays Does Not Increase during Anaphase

(A) Living embryos expressing *tetR-EGFP* and containing chromosomally integrated *tet*-operator-repeats were observed while progressing through mitosis 12 or 13. Images were acquired every 19 s. Single tetR-EGFP dots were selected and the background corrected intensities were determined.

(B) Intensities are plotted per tetR-EGFP dot. The graph represents data obtained from four embryos. For the five time points (145 s) after the metaphase-to-anaphase transition, which is the time frame when CID and CENP-C incorporation occurs, a total of 22–39 focused fluorescent dots were evaluated per time point. The fluorescence intensity of tetR-EGFP stays low after the metaphase-to-anaphase transition. Red arrows indicate the time points from which the sample images shown in (A) were taken. Data are presented as mean ± SD.

embryos in a halocarbon oil filled chamber sealed at the bottom with a gas-permeable membrane (YSI). For the FRAP analyses, a region of interest (ROI) was selected and the centromeric signals were bleached with four (Figure 2) or eight (Figure S3) pulses of the argon laser at 100% power. Images were acquired every 11.5 s (Figure 2) or every 3.9 s (Figure S3) after bleaching.

Quantitation of In Vivo Imaging Data

Quantitation of pixel intensities was performed with the software ImageJ (ver. 1.34n) (http://rsb.info.nih.gov/ij/index.html). For the determination of EGFP-CID and EYFP-CENP-C fluorescence intensities as shown in Figures 1A, 1C, and 3B, nuclear regions were identified in the red (chromatin) channel by a segmentation algorithm (Gaussian and anisotropic diffusion filtering [S13] followed by application of an appropriate threshold). These regions were used as ROIs to determine the mean pixel intensities and area of the accordingly segmented EGFP-CID or EYFP-CENP-C signals in the green channel per nucleus with the original unfiltered images. For background correction, cytoplasmic regions outside the chromatin areas were identified by segmentation, and the mean cytoplasmic pixel intensities in the green channel were subtracted from the mean centromeric pixel intensities. The absolute centromeric fluorescence intensities per nucleus were calculated by multiplying the background corrected mean centromeric pixel intensities with the number of evaluated pixels within the individual ROIs. In cases where the segmentation algorithm did not accurately assign ROIs for the individual centromere groups (particularly during prophase and early anaphase), ROIs were selected manually. For every time point in each experiment, the 10 or 5 (in case of one EYFP-CENP-C time series) highest values of corrected nuclear centromeric fluorescence intensity were selected and used to calculate a mean value per nucleus for this time point. The mean values per nucleus from three time series were aligned with the metaphase-to-anaphase transition as reference point, normalized to the first displayed time point in interphase, and mean values for the three series were calculated and plotted. The fluorescence intensities for His2Av-mRFP1 (Figure 1D and Figure S4) were determined in the red channel accordingly.

For the determination of EGFP-CID and EYFP-CENP-C fluorescence intensities after injection of colcemid as shown in Figure 3A, ROIs were selected manually and the background correction was performed as described above. The nuclei in colcemid injected embryos do not segregate their DNA, so the onset of chromosome condensation was used to align the data sets obtained from different embryos (four sets for $Mps1^{-/-}$ embryos and five sets for $Mps1^{+/+}$ embryos). While the centromeres are grouped in interphase at the apical surface of the nuclei, they redistribute rapidly throughout the nuclear space when the nuclei enter mitosis. Thus, our analysis of fluorescence intensities during the early stages of mitosis by means of single confocal planes did not permit the simultaneous evaluation of all centromere signals in the selected nuclei, resulting in a decrease of the measured intensities. This effect is exacerbated when no microtubules are present. The first data points displayed in Figure 3A were taken from nuclei in early mitosis, so the actual measured fluorescence intensity is lower than during the preceding interphase. Thus, the EGFP-CID fluorescence intensities for the $Mps1^{-/-}$ nuclei increase after progression through mitosis to values greater than twice the initial value displayed in the graph.

For the FRAP analyses (Figures 2 and S3), the background corrected centromeric pixel intensities for EGFP-CID and EYFP-CENP-C were determined as outlined above. The pixel intensities determined for the frame immediately before bleaching were normalized to one, and during recovery, the cumulative pixel intensities for all bleached centromeres were plotted. In the "regional" FRAP experiments (Figure S3), approximately 8 nuclei for each cell-cycle stage were bleached within a larger optical field and initial recovery of fluorescence at the centromeres was monitored. For background correction, the values of cytoplasmic pixels within the bleached regions were used. When only single metaphase plates were bleached within a very small ROI (Figure 2), the entire cytoplasmic region was used for determination of background pixel values. Data from three independent experiments were combined for the plots. For the plot shown in Figure 2B, only series were aligned in which bleaching took place two frames (~14 s) before the metaphase-to-anaphase transition.

For the determination of single centromere intensities of EGFP-CID (Figure 1B), in each frame every centromere that was in focus and not tightly clustered with other centromeres was selected with a circular ROI slightly larger than the centromere itself. The mean pixel intensity was calculated and background correction was performed by subtracting mean cytoplasmic fluorescence intensities determined as for the nuclear EGFP-CID fluorescence intensity evaluation (see above). Three independent time series were aligned with the metaphase-to-anaphase transition as reference point, normalized to the first displayed time point in interphase, and mean values for the series were calculated and plotted as intensity per centromere. Each data point represents the average intensity determined for a total of 50 to 200 individual centromeres. With the beginning of metaphase, the separate evaluation of sister centromeres results in an approximate 50% drop of the intensity per centromere. In late anaphase and telophase, the evaluation of single centromeres was

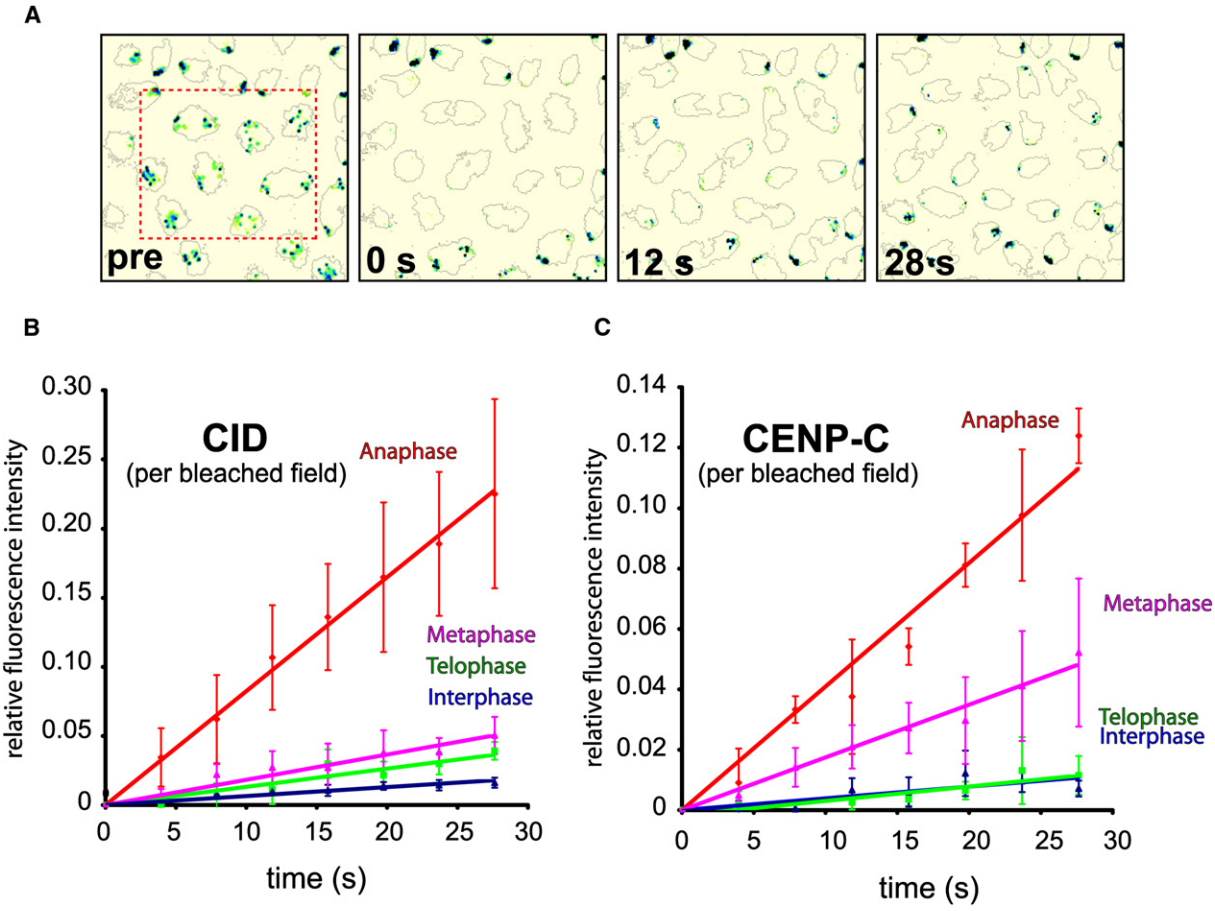

Figure S3. EGFP-CID and EYFP-CENP-C Are Most Dynamic during Anaphase

Living embryos expressing *His2Av-mRFP1* and *EGFP-cid* or *EYFP-Cenp-C* were observed while progressing through mitosis 12. During various cell-cycle stages, ROIs were selected and bleached with high laser power at 488 nm. The recovery of centromeric EGFP-CID and EYFP-CENP-C fluorescence was monitored.

(A) Example of a time-lapse series after bleaching of multiple mitotic figures during anaphase used for quantitation. EGFP-CID fluorescence is shown in dark green. The contours of the DNA masses of the dividing nuclei are indicated by fine gray lines.

(B and C) Initial FRAP dynamics for EGFP-CID (B) and EYFP-CENP-C (C) after bleaching were monitored. Data sets from three to four independent experiments were combined. The fluorescence intensity after bleaching was set to zero. Error bars indicate standard deviations. Only little recovery was obtained when EGFP-CID and EYFP-CENP-C were bleached during interphase, suggesting that both proteins are stably associated with the centromeres at this stage ([B], [C], blue curves). The slight recovery of fluorescence may be due to reversible photobleaching of GFP variants [S14]. Increased recovery rates of fluorescence were observed during mitosis. Quantitation during metaphase ([B], [C], pink curves) revealed that recovery rates were approximately three times as high as during interphase, suggesting increased turnover of both CID and CENP-C, as no considerable net incorporation was recorded during this phase. Significantly, highest recovery rates were recorded during anaphase ([B], [C], red curves). The initial rates do not support a full recovery during anaphase in contrast to the measurements with single bleached mitotic figures (Figure 2B), most probably because in the "regional" bleaching experiments, a significant fraction of bleached molecules derived from the larger bleached cytoplasmic pool surrounding the chromatin becomes incorporated. We could not perform half-life determinations because a recovery to saturation could not be obtained because of the short duration of anaphase of about only 90 s. Thus, the graphs in (B) and (C) represent the initial, approximately linear course of recovery rather than the exponential recovery curves typical for FRAP experiments. Data are presented as mean ± SD.

impossible because clustering of the signals resulting in a gap between the data points III and IV of Figure 1B. For a false color illustration, the lookup table "Fire" available with the ImageJ software was employed. The point-like signals of tetR-EGFP fusion proteins (Figure S2) were evaluated in an identical fashion as the single centromeres.

For the evaluation of EGFP-CID signal intensities in a *cid* mutant background (Figure S1), the segmentation algorithm could not be applied because no His2Av-mRFP1 was present. Instead, centromere groups that were in focus were selected manually and mean pixel intensities were calculated. For background correction, the mean pixel intensities of manually selected cytoplasmic regions were subtracted, which were determined for each frame.

For the quantitation of EGFP-CID fluorescence intensity during the postblastoderm mitoses 15 and 16, time-resolved z-stacks via the Leica DM-IRBE/TCS SP1 confocal system were recorded. In these later cycles, the cells do not divide synchronously in the same plane and the daughter nuclei often move perpendicular to the surface during cell division. Three slices, 0.7 μm apart, were recorded in 20 s intervals. Identification of centromere groups by segmentation and background correction were performed for every slice as described above. ROIs were defined and evaluated for metaphase and for anaphase figures in every slice. Only the highest of the three metaphase values and the highest of the six daughter anaphase values within the three z-slices for one dividing cell were used for calculating the mean fluorescence intensities. For comparison, the same recording and evaluation procedure was also used to measure fluorescence intensities during syncytial divisions. As a control for bleaching effects, an equal number of images were taken from a stage 11 embryo at short succession

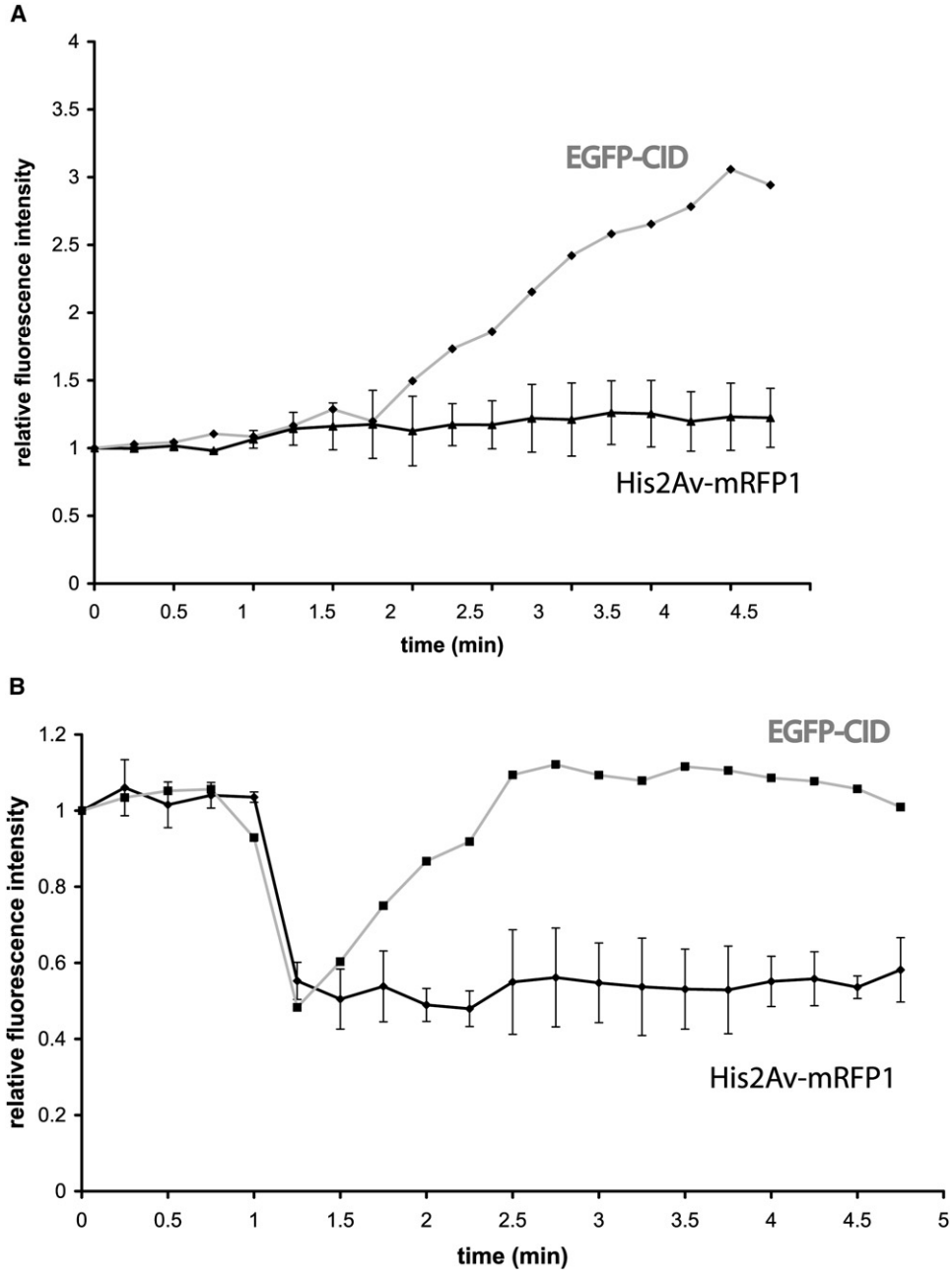

Figure S4. The Fluorescence Intensity of His2Av-mRFP1 Does Not Change during Mitosis when Colcemid Is Injected in Spindle Checkpoint-Deficient Embryos or when DNA Replication Is Inhibited

Living embryos expressing *His2Av-mRFP1* and *EGFP-cid* were observed while progressing through syncytial mitoses, and His2Av-mRFP1 fluorescence intensity was quantitated and plotted as in Figure 1D. Colcemid (A) or aphidicolin (B) were injected to inhibit spindle formation or DNA replication, respectively. Injected embryos were wild-type (B) or devoid of a functional spindle checkpoint because of the lack of the checkpoint kinase Mps1 (A). The gray lines in (A) and (B) indicate the fluorescence intensity changes of EGFP-CID as shown in Figure 3A (*Mps1*$^{-/-}$) and Figure 3B, respectively. The graphs represent average values obtained from 4 to 5 embryos. Data for His2Av-mRFP1 are presented as mean ± SD.

under identical conditions. The evaluation of the total fluorescence intensity revealed no significant reduction resulting from bleaching (<1%).

Aphidicolin (295 μM in 1% (v/v) DMSO) and colcemid (1 mM in 10% (v/v) DMSO) were injected laterally into the embryos. Time-lapse recordings started immediately after the injections. No anaphase resulting in separation of the sister centromeres occurred after colcemid injection, so intensities were determined for the total centromere-localized fluorescence per nucleus throughout the experiment.

Supplemental References

S1. Kalitsis, P., Fowler, K.J., Earle, E., Griffiths, B., Howman, E., Newson, A.J., and Choo, K.H. (2003). Partially functional Cenpa-GFP fusion protein causes increased chromosome missegregation and apoptosis during mouse embryogenesis. Chromosome Res. *11*, 345–357.

S2. Malik, H.S., Vermaak, D., and Henikoff, S. (2002). Recurrent evolution of DNA-binding motifs in the *Drosophila* centromeric histone. Proc. Natl. Acad. Sci. USA *99*, 1449–1454.

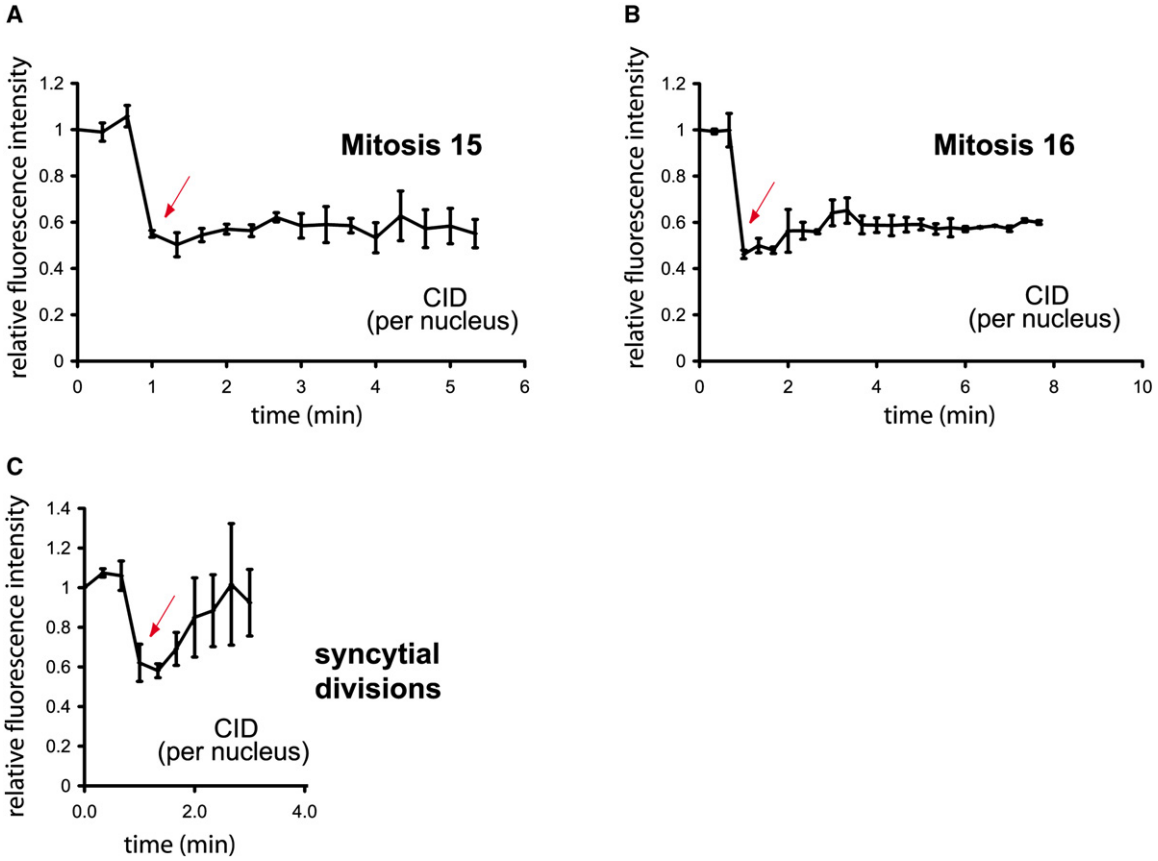

Figure S5. EGFP-CID Is Not Incorporated into Centromeres during the Postblastoderm Mitoses 15 and 16

Living embryos expressing *EGFP-cid* and *His2Av-mRFP1* were observed while progressing through epidermal mitosis 15 (A), 16 (B), and the syncytial mitoses 12 or 13 (C). Z-stacks (3 planes, 0.7 μm apart) were recorded every 20 s. Fluorescence intensities of EGFP-CID were determined for selected nuclei in each image. Only the highest value for a certain nucleus obtained from one of the three planes within a z-stack was used to calculate the intensity at a specific time point. The mean intensities of centromeric EGFP-CID fluorescence are plotted as relative intensities per nucleus. Beginning at the onset of anaphase (red arrows), segregating sister centromere groups were evaluated separately, resulting in an approximately 50% intensity drop. Data sets from three embryos were combined. Although the fluorescent intensities after progressing through mitoses 15 and 16 remained at the level of approximately 50% for at least 5 min (A, B), it increased rapidly when nuclei in syncytial embryos were observed under the same conditions (C). Data are presented as mean ± SD.

S3. Horn, C., and Wimmer, E.A. (2000). A versatile vector set for animal transgenesis. Dev. Genes Evol. *210*, 630–637.

S4. Pirrotta, V. (1988). Vectors for P-element transformation in *Drosophila*. In Vectors: A Survey of Cloning Vectors and Their Uses, R.L. Rodriguez and D.T. Denhardt, eds. (Boston: Butterworths), pp. 437–456.

S5. Campbell, R.E., Tour, O., Palmer, A.E., Steinbach, P.A., Baird, G.S., Zacharias, D.A., and Tsien, R.Y. (2002). A monomeric red fluorescent protein. Proc. Natl. Acad. Sci. USA *99*, 7877–7882.

S6. Clarkson, M., and Saint, R. (1999). A His2AvDGFP fusion gene complements a lethal His2AvD mutant allele and provides an in vivo marker for *Drosophila* chromosome behavior. DNA Cell Biol. *18*, 457–462.

S7. Michaelis, C., Ciosk, R., and Nasmyth, K. (1997). Cohesins: chromosomal proteins that prevent premature separation of sister chromatids. Cell *91*, 35–45.

S8. Tracey, W.D., Jr., Ning, X., Klingler, M., Kramer, S.G., and Gergen, J.P. (2000). Quantitative analysis of gene function in the *Drosophila* embryo. Genetics *154*, 273–284.

S9. Blower, M.D., Daigle, T., Kaufman, T., and Karpen, G.H. (2006). *Drosophila* CENP-A mutations cause a BubR1-dependent early mitotic delay without normal localization of kinetochore components. PLoS Genet. *2*, e110. 10.1371/journal.pgen.0020110.

S10. Heeger, S., Leismann, O., Schittenhelm, R., Schraidt, O., Heidmann, S., and Lehner, C.F. (2005). Genetic interactions of separase regulatory subunits reveal the diverged *Drosophila* Cenp-C homolog. Genes Dev. *19*, 2041–2053.

S11. Fischer, M.G., Heeger, S., Häcker, U., and Lehner, C.F. (2004). The mitotic arrest in response to hypoxia and of polar bodies during early embryogenesis requires *Drosophila* Mps1. Curr. Biol. *14*, 2019–2024.

S12. Pandey, R., Heidmann, S., and Lehner, C.F. (2005). Epithelial re-organization and dynamics of progression through mitosis in *Drosophila* separase complex mutants. J. Cell Sci. *118*, 733–742.

S13. Black, M.J., Sapiro, G., Marimont, D.H., and Heeger, D. (1998). Robust anisotropic diffusion. IEEE Trans. Image Process. *7*, 421–432.

S14. Sinnecker, D., Voigt, P., Hellwig, N., and Schaefer, M. (2005). Reversible photobleaching of enhanced green fluorescent proteins. Biochemistry *44*, 7085–7094.